Received: 11 September 2017 | Accepted: 12 March 2018

DOI: 10.1111/jmg.12310

ORIGINAL ARTICLE

WILEY Journal of METAMORPHIC GEOLOGY

Deep komatiite signature in cratonic mantle pyroxenite

Dirk Spengler[1,2] | Herman L.M. van Roermund[2] | Martyn R. Drury[2]

[1]Institut für Mineralogie und Kristallchemie, Universität Stuttgart, Stuttgart, Germany

[2]Faculteit Geowetenschappen, Universiteit Utrecht, Utrecht, The Netherlands

Correspondence
Dirk Spengler, Institut für Mineralogie und Kristallchemie, Universität Stuttgart, Stuttgart, Germany.
Email: spengler@geo.uni-potsdam.de

Handling editor: Doug Robinson

Abstract

We present new and compiled whole-rock modal mineral, major and trace element data from extremely melt depleted but pyroxenite and garnet(-ite)-bearing Palaeoarchean East Greenland cratonic mantle, exposed as three isolated, tectonically strained orogenic peridotite bodies (Ugelvik, Raudhaugene and Midsundvatnet) in western Norway. The studied lithologies comprise besides spinel- and/or garnet-bearing peridotite (dunite, harzburgite, lherzolite) garnet-clinopyroxenite and partially olivine-bearing garnet-orthopyroxenite and -websterite. Chemical and modal data and spatial relationships between different rock types suggest deformation to have triggered mechanical mixing of garnet-free dunite with garnet-bearing enclosures that formed garnet-peridotite. Inclusions of olivine in porphyroclastic minerals of pyroxenite show a primary origin of olivine in olivine-bearing variants. Major element oxide abundances and ratios of websterite differ to those in rocks expected to form by reaction of peridotite with basaltic melts or silica-rich fluids, but resemble those of Archean Al-enriched komatiite (AEK) flows from Barberton and Commondale greenstone belts, South Africa. Websterite Gd_N/Yb_N, 0.49–0.65 (olivine-free) and 0.73–0.85 (olivine-bearing), overlaps that of two subgroups of AEK, Gd_N/Yb_N 0.25–0.55 and 0.77–0.90, with each of them being nearly indistinguishable from one another in not only rare earth element fractionation but also concentration. Websterite MgO content is high, 22.7–29.0 wt%, and Zr/Y is very low, 0.1–1.0. The other, non-websteritic pyroxenites overlap—when mechanically mixed together with garnetite—in chemistry with that of AEK. It follows an origin of websterite and likely all pyroxenite that involves melting of a garnet-bearing depleted mantle source. Pyroxene exsolution lamellae in the inferred solidus garnet in all lithological varieties require the pyroxenites to have crystallized in the majorite garnet stability field, at 3–4 GPa (90–120 km depth) at minimum 1,600°C. Consequently, we interpret the websterites to represent the first recognized deep plutonic crystallization products that formed from komatiite melts. The other pyroxenitic rocks are likely fragments of such crystallization products. An implication is that a mantle plume environment contributed to the formation of (one of) the worldwide oldest lithospheric mantle underneath the eastern Rae craton.

KEYWORDS

Archean, cratonic mantle, garnet-pyroxenite, komatiite, pyroxene exsolution

1 | INTRODUCTION

Archean cratons are believed to represent the first landmasses that resisted tectonic recycling into the mantle. The reason is the exceptional buoyancy of the underlying, more than 200 km thick, lithospheric mantle that records up to 50% melt depletion (Herzberg, 2004; Pearson & Wittig, 2008; Walter, 2003). The geodynamic environment responsible for the melting giving rise to this depletion—mantle plume, spreading centre or subduction zone—and thus plate tectonics' involvement remains, however, highly controversial (Arndt, Coltrice, Helmstaedt, & Gregoire, 2009; Herzberg & Rudnick, 2012). Assessing the melting depth and temperature and by inference the geodynamic regime of melting based on the residual chemistry of natural peridotite samples is problematic. One difficulty relates to the high degree of melt extraction that produces residua free of clinopyroxene and garnet, the two phases most commonly used as proxies of the melting pressure (Pearson & Wittig, 2008). Once both minerals have partitioned into the melt, the geochemistry of residua is virtually pressure insensitive. Furthermore, residua are susceptible to re-enrichments in melt-compatible elements, mainly Fe, Al and Si, that commonly have overprinted primary chemical signatures (Simon, Carlson, Pearson, & Davies, 2007).

Our approach is to constrain the peridotite melting regime from the chemistry of pyroxenites enclosed in cratonic mantle fragments in the Western Gneiss Region of Norway. Isolated peridotite outcrops (Ugelvik, Raudhaugene, Midsundvatnet) in a 15 × 6 km^2 of Otrøy Island vary in size from 100 to 1,000 m, and are recognized as lithospheric mantle fragments from the East Greenland Rae craton (St-Onge, Van Gool, Garde, & Scott, 2009) that became incorporated into the Baltic Shield during the Caledonian orogeny (Brueckner, 1998; Spengler, Brueckner, van Roermund, Drury, & Mason, 2009; Van Roermund, Drury, Barnhoorn, & De Ronde, 2000). The orogenic peridotites are compositionally layered. Individual layers vary in thickness from a few mm to a few m. Petrographic field mappings showed them to consist (in approximate proportions) of dunite (10%), spinel-dunite (50%), garnet-harzburgite/dunite (30%) and garnet-spinel-harzburgite/dunite (10%; Spengler, 2006; Van Roermund et al., 2000). Peridotite layers containing clinopyroxene of more than 5% (garnet-lherzolite, <1%) rarely exceed a few mm in thickness. Layers and lenses of garnet-pyroxenite (<1%) occur locally concentrated and can be subdivided into garnet-clinopyroxenite (20%) and partially olivine-bearing garnet-websterite (70%). Some pyroxenites show extreme modal compositions in the form of garnet-(olivine-)orthopyroxenite (10%; Carswell, 1973) and garnetite (<1%; Van Roermund & Drury, 1998). The outcrop form of the pyroxenitic rocks is variable, but detailed mapping established deformation is the major control: individual layers are locally tightly folded and can be mapped for up to 300 m. Thicknesses of pyroxenite layers and lenses vary by orders of magnitude, a few mm to 1 m. Individual minerals in all rock types range in size from sub-mm in samples deformed during the latest tectono-thermal event to several cm in samples that record minimal deformation and retain Meso- and Palaeoarchean isotopic ages (Spengler, 2006; Spengler et al., 2009). Locally, pre-Caledonian garnet in all lithologies contains pyroxene lamellae that formed by exsolution from former majorite garnet (Spengler et al., 2009; Van Roermund & Drury, 1998).

In this study, we present field relationships between different mantle lithologies and the mineralogy, petrology and whole-rock geochemistry of 10 pyroxenite and 10 peridotite samples. Our data set has been enlarged by the addition of data from previous studies: three samples were added to the pyroxenite subset (Carswell, 1973; Spengler, 2006; Spengler et al., 2006) and 12 to the peridotite subset (Spengler, 2006). The full set of 12 pyroxenite and 22 peridotite samples is used to infer the melting–crystallization conditions of the three peridotite bodies; their locations are shown in Figure 1.

2 | METHODS

Major elements: Whole-rock samples were powdered using agate moulds. Powders were mixed with Li-borates, molten to glass tablets and subsequently analysed for major element oxides using X-ray fluorescence techniques at Utrecht University (Bruker SRS 3400) and at Vrije Universiteit Amsterdam. The oxides in sample EZ108 were determined from a powder-pressed pellet. Mineral modes were calculated using a least squares method from whole-rock analyses in combination with mineral compositions (Table S3) measured by electron microprobe at Utrecht University (JEOL JXA8600), at Vrije Universiteit Amsterdam (JEOL JXA8800M) and at Stuttgart University (Cameca SX100). Analytical conditions were 15 kV acceleration voltage, 15–25 nA beam current, 0–1 μm spot size, 20–50 s peak counting in WDS mode. Obtained data were corrected using the ZAF routine. External calibration occurred against international oxide and silicate standards with a precision of 0.5–1%.

Trace and rare earth elements (REE): Whole-rock powders (∼100 mg) were dissolved in HNO_3 at low-dilution factors between 1:150 and 1:250 and analysed by solution inductively coupled plasma mass spectrometry (ICP-MS) using an Agilent 7500 at TNO Utrecht and a HP 4500plus system at Vrije Universiteit Amsterdam. The USGS reference material DTS-1 was reproduced within 3–20%, except

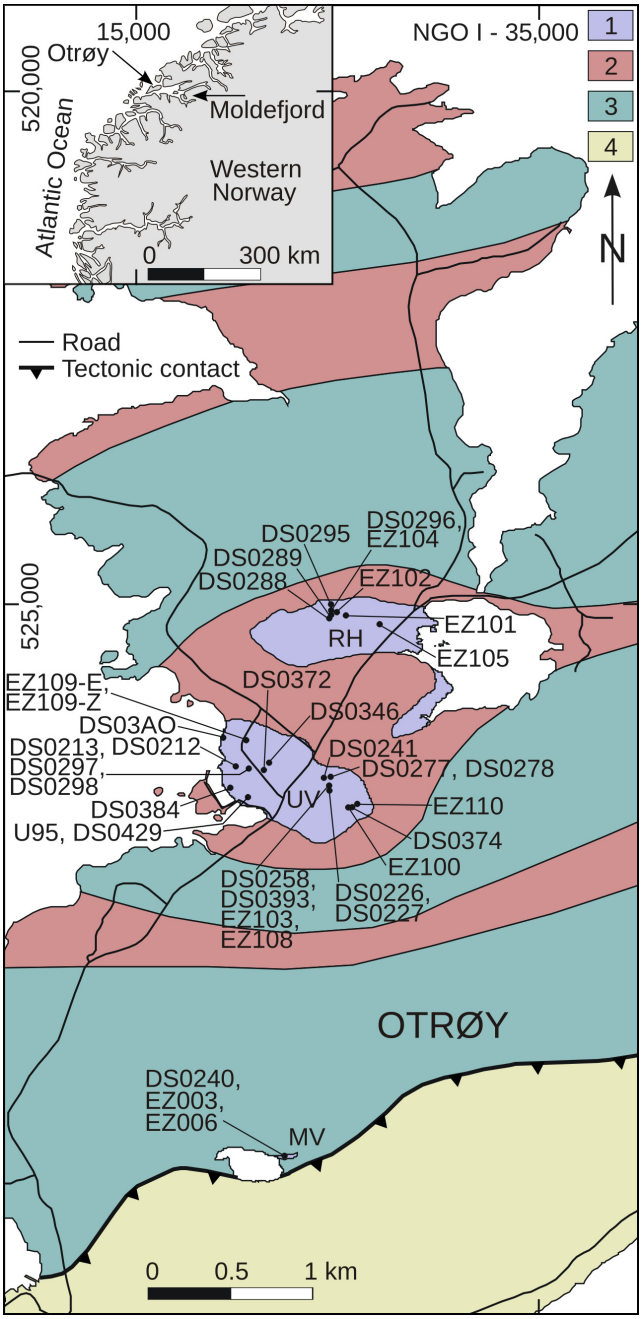

FIGURE 1 Simplified geological map of western Otrøy island (modified after Carswell, Van Roermund, & Wiggers de Vries, 2006) that shows the position of samples and of orogenic peridotite bodies (1; MV—Midsundvatnet, RH—Raudhaugene, UV—Ugelvik) embedded in gneiss (2—banded dioritic gneiss with abundant eclogite, 3—migmatitic or augen gneiss with minor eclogite, 4—granitoid gneiss and metasediment). The inset locates the study area in western Norway

for Tb, 33%. The trace and REE composition of sample DS0429—that is, a fragment of a m-sized garnet-orthopyroxenite lens U95 described by Carswell (1973)—were calculated from mineral modes in combination with mineral compositions (Table S4) measured by laser ablation ICP-MS (Agilent 7500S ICP-MS platform, MicroLas GeoLas Q-plus laser microsampler, 193 nm ArF excimer) at Kanazawa University under conditions described in Spengler et al. (2012).

3 | RESULTS

3.1 | Petrography

Peridotite in all three mantle bodies has olivine that is partially sepentinized, ~50%. Individual olivine crystals are typically sub-mm to mm in size. Dunite layers at Ugelvik and Raudhaugene occasionally preserve cm-scale fragments (porphyroclasts) of olivine up to 10 cm in size (Figure 2a). Variable proportions of orthopyroxene, clinopyroxene, spinel and garnet define the compositional layering in peridotite and often occur concentrated in distinct horizons (Figures 2b and 3b). Calculated mineral modes vary for samples from Ugelvik and Raudhaugene with olivine 55–99 wt%, orthopyroxene 0–14 wt%, clinopyroxene 0–15 wt%, spinel 0–1 wt% and garnet 0–35 wt% (Table S2). Garnet-free peridotite of the sample suite is solely dunitic in composition, petrographically and chemically, and partially contains minor kelyphite up to a few mm in diameter after former garnet. The garnet-bearing variants cover the range of dunite, harzburgite and lherzolite. Single grains of garnet in peridotite are predominantly a few mm in size, but occasionally exceed 1 cm as porphyroclasts (Figure 2b). The latter frequently enclose sub-mm-sized grains of orthopyroxene, clinopyroxene or olivine. Peridotite from the Midsundvatnet body has not been included in this study.

All three peridotite bodies enclose pyroxenitic lithologies that usually have sharp contacts with parallel orientation to the compositional peridotite layering. At Midsundvatnet, the pyroxenites form only discrete layers (Figure 3), low-strain megacrystic mineral assemblages have not been observed. These pyroxenite samples are garnet-olivine-websterite in composition. Porphyroclastic garnet is typically a few mm in size and has inclusions of granular olivine (Figure 4a) apart from areas containing exsolved lamellar pyroxenes and Ti-oxide (Figure 4c). These garnet porphyroclasts occur within near equigranular textures of recrystallized grains that are sub-mm to mm in size (Figure 4a). Calculated mineral modes range for olivine 30–35 wt%, orthopyroxene 21–27 wt%, clinopyroxene 25–27 wt% and garnet 15–18 wt% (Table S1). Individual layers are partially discontinuous and grade into garnet-peridotite (Figure 3).

More lithological variety of pyroxenite occurs in the two large peridotite bodies Ugelvik and Raudhaugene, where the enclosed pyroxenites form layers and lenses. The layered type pyroxenites include garnet-websterite

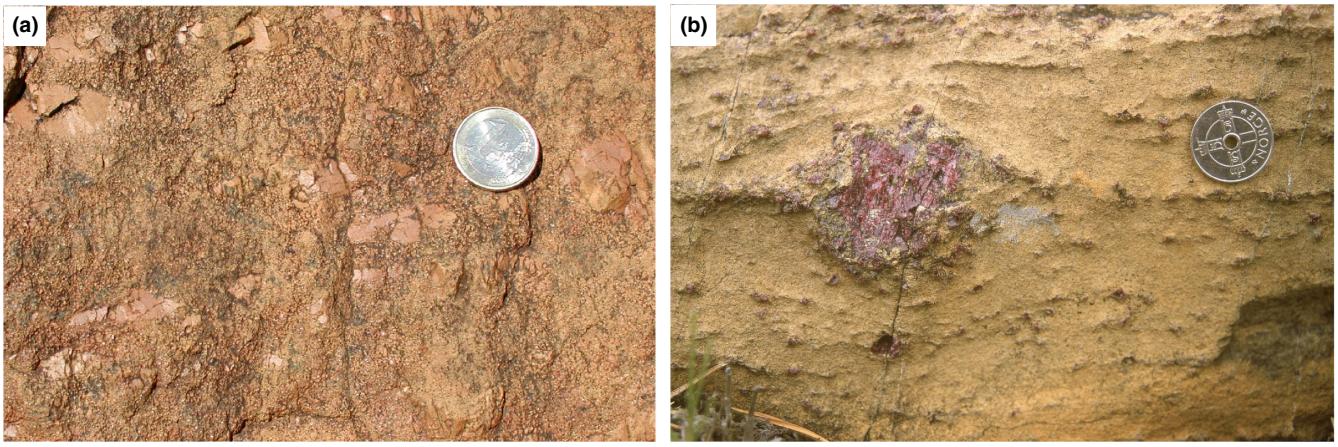

FIGURE 2 Field photographs of coarse mineral fragments in dynamically recrystallized peridotite at Ugelvik. (a) Subhorizontal elongated cm-sized fragments of olivine in fine dynamically recrystallized dunite. (b) Garnet–peridotite that contains a porphyroclastic nodule of polycrystalline garnet (or garnetite). Defragmented garnet grains (and minor dynamically recrystallized garnet grains) form the tails centre-aligned parallel to the compositional layering that otherwise bends around the porphyroclast. Other finely distributed garnet fragments occur concentrated in horizons. Coin 2 cm

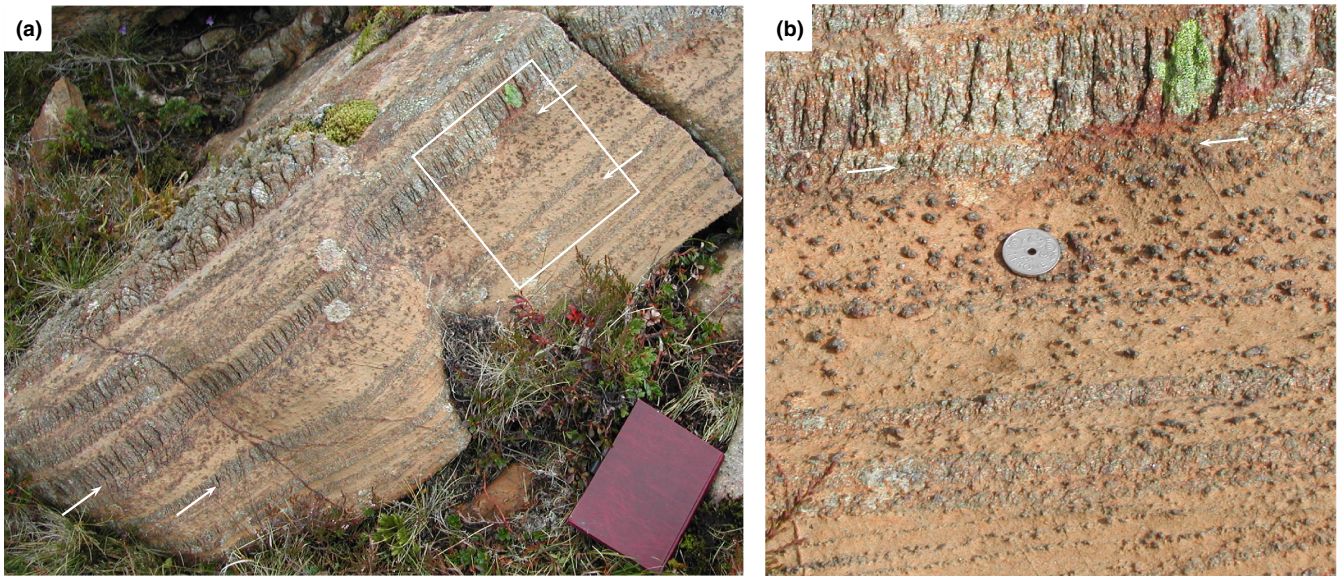

FIGURE 3 Field photographs of garnet–olivine–websterite in peridotite at Midsundvatnet. (a) Continuous websterite layers with cm-scale thickness and typical fractures subvertical to the layering (arrows on the left) are partially thinned, disrupted and mixed with peridotite (arrows on the right). (b) Close-up photo of the area with square outline in (a). Fragments of websterite in peridotite form garnet-peridotite (image centre) and discrete layers of garnet–peridotite in alternation with garnet-free peridotite (bottom). Objects for scale: book 13 cm × 18 cm, coin 2 cm

(orthopyroxene 32–46 wt%, clinopyroxene 39–40 wt%, garnet 15–29 wt%), garnet-clinopyroxenite (clinopyroxene ~35 wt%, garnet ~65 wt%) and garnet-olivine-orthopyroxenite (olivine 42 wt%, orthopyroxene 50 wt%, clinopyroxene 3 wt%, garnet 5 wt%). These layers are dynamically recrystallized as evident from shape preferred orientations of minerals, enclosed porphyroclasts of garnet and orthopyroxene and crystal–plastic deformation microstructures in the latter (Figure 4b). Olivine-bearing layers have orthopyroxene crystals up to a few cm in size with olivine inclusions (Figure 4b). Matrix minerals are sub-mm to mm in grain size. In contrast, lenses (or nodules if a few cm in diameter; Figure 2b) have individual crystals up to several cm in size, that is, one to two orders of magnitude larger than that of dynamically recrystallized grains in peridotite and pyroxenite. The megacrystic mineral assemblages are garnet-orthopyroxenite and garnetite, record low or no deformation and have been described earlier (Carswell, 1973; Spengler et al., 2006; Van Roermund & Drury, 1998).

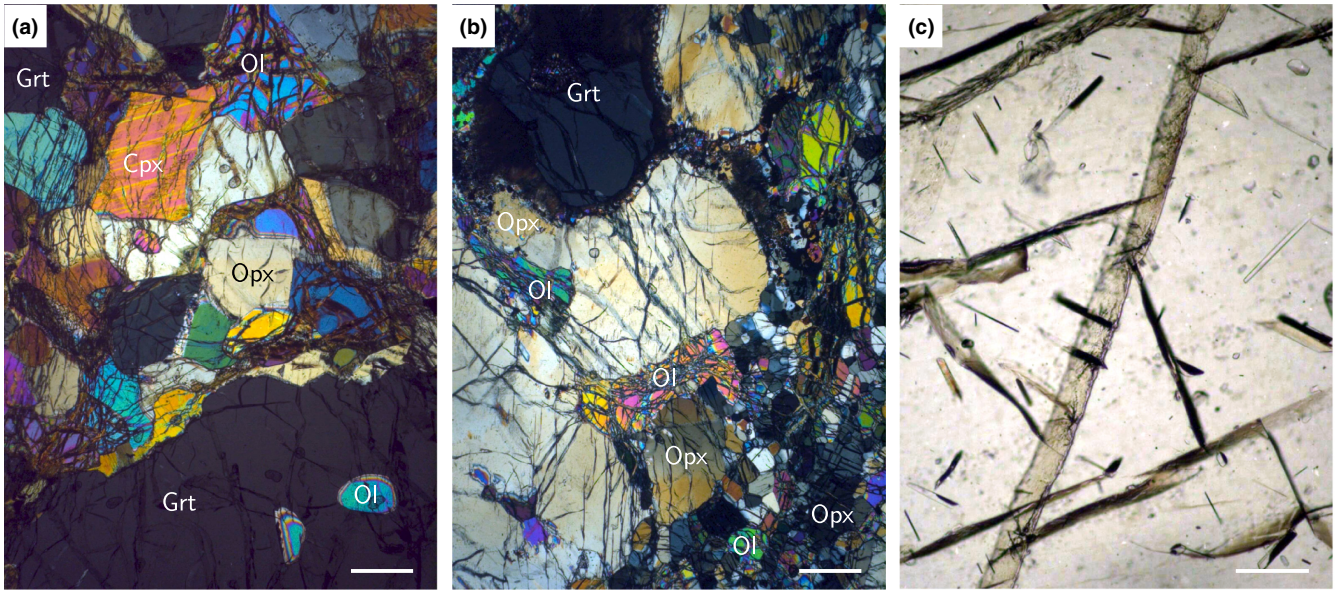

FIGURE 4 Micrographs of olivine-bearing pyroxenite. (a) Garnet–olivine–websterite (sample DS0240) shows porphyroclastic garnet with olivine inclusions (lower part of the image) next to recrystallized matrix grains of olivine, orthopyroxene, clinopyroxene and garnet (upper part, nearly cross-polarized light). (b) Garnet–olivine–orthopyroxenite (sample DS0372) has porphyroclastic orthopyroxene with undulose extinction and inclusions of olivine and garnet partially replaced by secondary minerals (left side). The recrystallized matrix (right side) is composed of orthopyroxene, olivine, replacements after garnet, minor clinopyroxene and oxides (nearly cross-polarized light). (c) A porphyroclastic garnet core (sample DS0240) shows acicular to lamellar inclusions of Ti-oxide (dark, thin), of pyxoxene (bright, thicker) and of both phases together (bi-coloured) with an apparent orientation towards 1 o'clock, 4 o'clock and 5 o'clock (plane-polarized light). The inclusions' visible length does not exceed that of the scale bar. Linear structures across half or the entire image are cracks. Scale bars: 500 μm (a and b) and 100 μm (c). Abbreviations for mineral names follow the recommendation of Kretz (1983)

Garnet in all studied samples is purple to red in colour with the exception of the garnet-olivine-websterite sample DS0372 that has dark green garnet. The latter is characteristic for local Ca–Cr–Fe metasomatism and lacks evidence for lamellae microstructures (Spengler, 2006).

3.2 | Major and trace elements

Peridotite whole-rock compositions have atomic Mg/(Mg+Fe) ($Mg^{\#}$) that are highest for spinel-dunite, 0.92–0.94, intermediate and similar for garnet-dunite, 0.92, and garnet-harzburgite, 0.92–0.93, and lowest for garnet-lherzolite, 0.90–0.92. The powdered fraction of an olivine-megacryst nearly 10 cm in size has a $Mg^{\#}$ of 0.93. When displayed against calculated modal olivine, the peridotite compositions of the two large peridotite bodies then form a narrow interval within a mechanical mixing array between spinel-peridotite and all major garnet-bearing aluminous enclosures, $Mg^{\#}$ 0.76–0.89, of the same peridotite bodies (Figure 5a). Garnet-orthopyroxenite contrasts with a higher $Mg^{\#}$ of 0.93. The three websterite samples from the Midsundvatnet body have low $Mg^{\#}$, 0.82–0.84, and plot below the array.

A similar relationship is shown by a bivariate plot of the MgO/SiO_2 ratio against SiO_2 content, where garnet-peridotite clusters in between spinel-peridotite and major garnet-bearing pyroxenites (Figure 5b). MgO contents are high for all garnetite and pyroxenite samples, 17.1–38.7 wt%. Those of websterite composition lay within the range of that of komatiite sensu stricto (18–30 wt%; Arndt & Lesher, 2005).

Pyroxenite and garnetite have approximately one order of magnitude range in the contents of Al_2O_3, 1.3–23.5 wt%, and TiO_2, 0.03–0.45 wt% (Figure 6b). Their Al_2O_3/TiO_2 ratio differs between the different bodies and is lowest in the samples from Midsundvatnet, 19.5–27.9, and highest in the other two bodies, 29.6–470.4, except for the metasomatic sample DS0372, 24.2 (Figure 6b–d). In contrast, the CaO/Al_2O_3 ratio of non-peridotitic samples, 0.2–2.6, overlap in range between different bodies (Figure 6d). The Cr content of non-peridotitic samples range with approximately one order of magnitude, 407–8,533 μg/g, and is specific to rock type (Figure 7a). The Cr–Ti systematics show that garnet-peridotite clusters along a hypothetical mixing line between spinel-peridotite and garnet-websterite (Figure 7a). The Zr and Y contents in the pyroxenites range by two orders of magnitude, 0.153–15.6 μg/g and 0.114–22.7 μg/g respectively. Among these, the websterites show a correlation between Zr content and Zr/Y ratio, whereas such a relationship is not evident from the other pyroxenites and garnetite (Figure 7b). The total variation of Zr/Y in pyroxenite is 0.10–2.05 with the

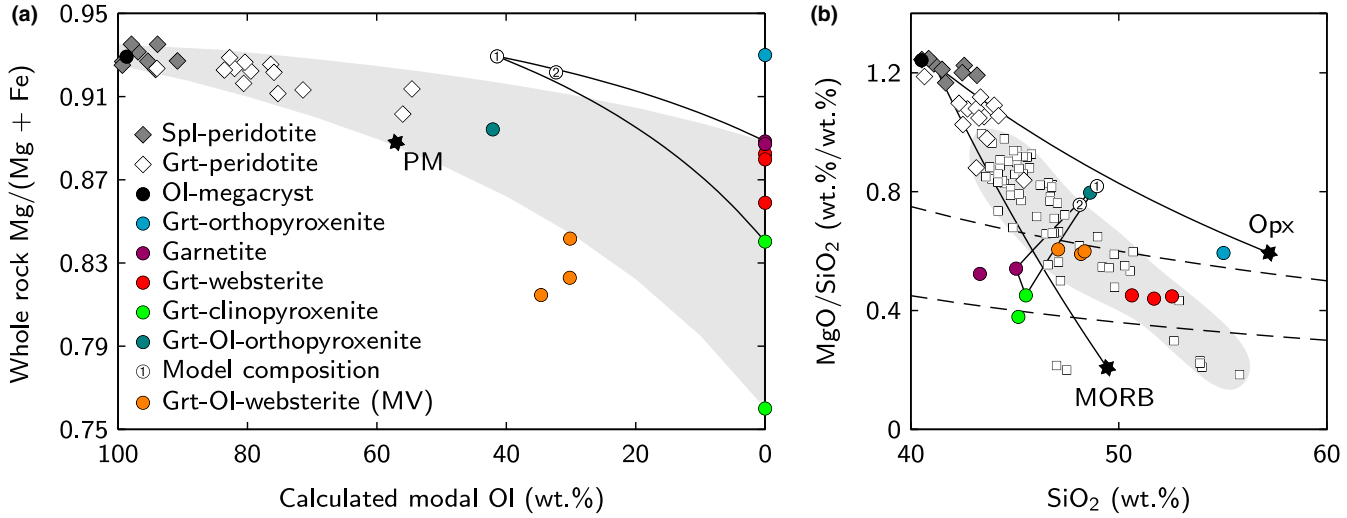

FIGURE 5 Whole-rock data from the Otrøy peridotite bodies show mixing relationships. (a) Atomic Mg/(Mg+Fe) *v.* calculated olivine mode. Ugelvik and Raudhaugene garnet-peridotites lay within an array (shaded) defined by mechanical mixing of garnet-free peridotite with different types of aluminous rocks. Solid lines represent bivariate mixing lines of selected end-members. Primitive mantle (PM) is from Sun (1982). MV, Midsundvatnet. (b) MgO/SiO_2 *v.* SiO_2 (colour code as in a). Otrøy garnet-websterite and South African komatiite flows (small squares; Hoffmann & Wilson, 2017; Robin-Popieul et al., 2012; Thompson Stiegler et al., 2010; Wilson, 2003) form a narrow array (shaded) that contrasts to mixing lines (solid) between dunite and an average Archean mid-ocean ridge melt (MORB; Komiya, Maruyama, Hirata, Yurimoto, & Nohda, 2004) and products formed by SiO_2-rich fluids (orthopyroxene; Simon et al., 2007). Dashed lines separate compositions with MgO of 18 wt% (lower) and 30 wt% (upper). Abbreviations for mineral names follow the recommendation of Kretz (1983)

lowest values occurring in olivine-free garnet-websterite, 0.10–0.15.

3.3 | Rare earth elements

The olivine-bearing websterite has moderately fractionated heavy REE, Gd_N/Yb_N 0.73–0.85, the olivine-free variant has lower ratios, 0.49–0.65, both at REE contents similar to or below that of primitve mantle (PM; Figure 6a). Orthopyroxene-rich pyroxenite also has low Gd_N/Yb_N, 0.38–0.47, but at element concentrations of one to two orders of magnitude below that of PM. Garnetite shows the strongest fractionation, 0.15–0.17, and clinopyroxenite the most variable, 0.58–1.33 at super-PM concentrations.

The olivine-megacryst also shows low Gd_N/Yb_N of 0.27, but the Gd content is close to the detection limit and so the measured ratio may likely be a maximum value. REE fractionation and concentration in peridotite depend on the peridotite mineralogy. Concentrations in spinel-peridotite range within about two to three orders of magnitude below that of PM. Higher the garnet mode, higher the whole-rock heavy REE content, up to super-PM values in sample DS0226.

4 | DISCUSSION

4.1 | Origin of garnet in peridotite

Recognition of the relationship between the different rock types is essential to assess the melting history that produced the peridotites and hence the tectonic setting of formation. Samples from the Ugelvik and Raudhaugene bodies cover a wide compositional variation (Figure 5). Whole-rock $Mg^{\#}$ and calculated olivine mode correlate with each other suggesting that garnet-peridotite ($Mg^{\#}$ 0.90–0.93) formed by mechanical mixing of garnet-free and garnet-bearing lithologies, that is, spinel-dunite ($Mg^{\#}$ 0.92–0.94) and garnet-clinopyroxenite, -websterite and garnetite ($Mg^{\#}$ 0.76–0.89). Garnet-orthopyroxenite differs in $Mg^{\#}$ for a given olivine mode and therefore may have played a minor role for admixing of garnet into peridotite. However, garnet-orthopyroxenite may likely have provided orthopyroxene to become concomitantly admixed into spinel-dunite to form layers of spinel-harzburgite that has not been included in the sample set. A mixing process is also indicated by field relationships in all three bodies where pyroxenite bands and spinel-peridotite occur highly sheared and peridotite with modal garnet gradients formed locally in between (Figure 3). Evidence for intense shear to have pervasively effected all peridotite bodies is documented by the widespread occurrence of porphyroclasts at macro- and microscopic scales (Figures 2 and 4).

A detailed examination of peridotite chemistry further supports a mixing model. Spinel-peridotites contain <1 wt% spinel, are virtually clinopyroxene-free dunites and are highly magnesian (median MgO 50.6 wt%) with low iron content (median FeO 6.8 wt%). When compared with experimental data, these compositions indicate an extracted melt fraction of 0.40 and 0.55, for adiabatic fractional

melting from 5 to 1 GPa (Herzberg, 2004) and batch melting at 5 GPa (Walter, 2003), respectively. In contrast, garnet-peridotite has highly variable modes of garnet (2–35 wt%) and clinopyroxene (0–15 wt%). The range of the whole-rock major element compositions, for example, MgO (38.0–48.5 wt%) and FeO (6.4–7.6 wt%), covers a large proportion of residual compositions produced experimentally over a wide range of pressure and temperature conditions (Herzberg, 2004; Walter, 2003) and therefore does not allow meaningful melt fractions to be estimated. In addition, the garnet/clinopyroxene ratio in peridotite is above unity. A residual origin of this ratio requires the partitioning of clinopyroxene over garnet into the melt at high pressures, but both minerals hardly remain in peridotite after a minimum 40% melt extraction (Herzberg, Condie, & Korenaga, 2010). Field relationships and rock chemistry suggest garnet and clinopyroxene in peridotite to be derived from an aluminous source. It is concluded that the origin of garnet in Otrøy peridotite is related to all major garnet-bearing pyroxenites and garnetite.

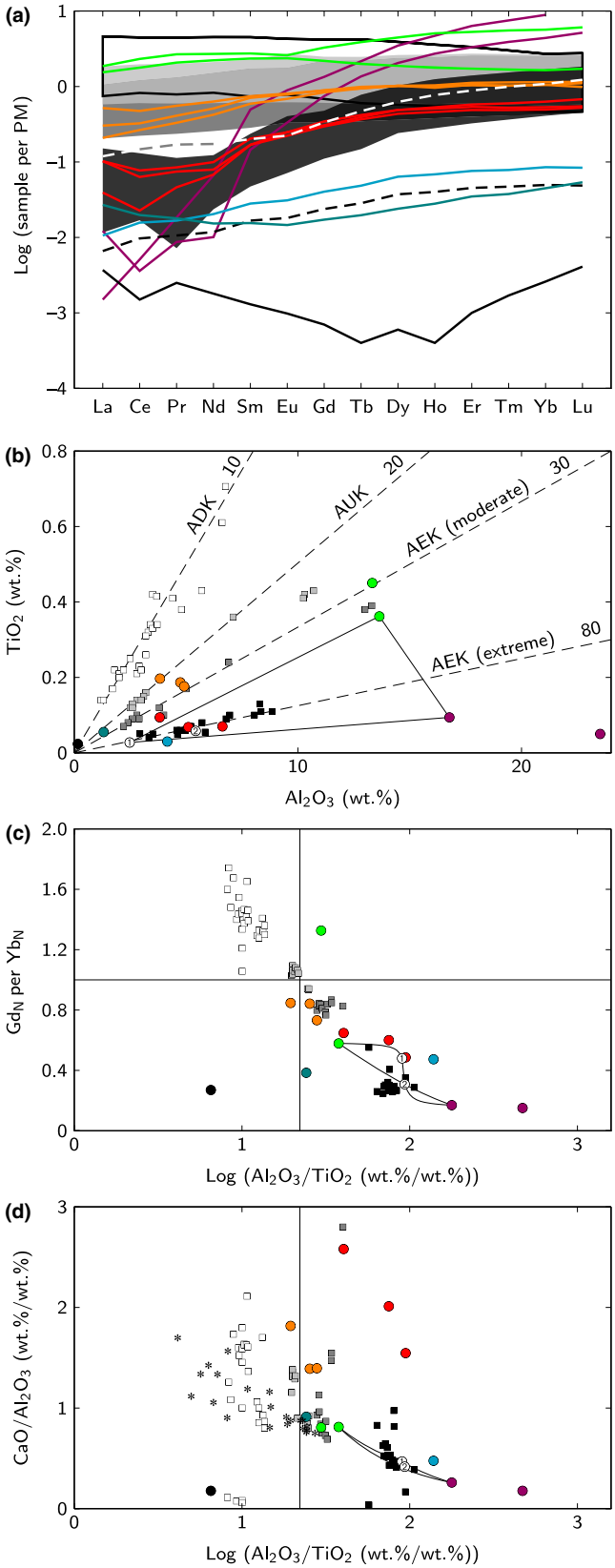

FIGURE 6 Whole-rock chemistry of Otrøy pyroxenite and garnetite (lines, dots; colour code as in Figure 5) and of South African komatiite flows (fields, squares; Hoffmann & Wilson, 2017; Robin-Popieul et al., 2012; Thompson Stiegler et al., 2010; Wilson, 2003). Shading for fields (a) and squares (b–d): no shade/white for Al_2O_3/TiO_2 8–14 (ADK), light grey for 20–25 (AUK), dark grey for 28–40 and black for 58–106 (moderate and extreme AEK respectively). REE were normalized to primitive mantle (PM) of Sun and McDonough (1989). Strongly re-enriched light REE of two Commondale samples (COM01/18 and COM01/19) were omitted for clarity. (a) REE concentrations of Otrøy websterite overlap those of AEK. Model compositions are shown as dashed lines (black for #1, white for #2). (b) TiO_2 and Al_2O_3 contents of Otrøy websterite overlap those of AEK. Dashed lines show selected oxide ratios typical for different komatiite subtypes (labelled). Solid lines denote the compositional variation in a hypothetical mixture of selected Ugelvik and Raudhaugene samples. (c) PM compositional ratios (lines; McDonough & Sun, 1995; Sun & McDonough, 1989) separate Al-depleted (upper left quadrant) from Al-enriched rocks (lower right). (d) High pressure (3–7 GPa) experimental batch melts of PM KR-4003 (asterisks; Walter, 1998) reproduce chemical ratios found in ADK and partially AUK (diagram's left side), but differ to those of AEK (right side). Compositional variation in Otrøy websterite overlaps that of AEK

4.2 | Pyroxenite model compositions

Garnet-olivine-orthopyroxenite DS0372 is the sample in the suite that has by far the highest Cr content (8,533 μg/g) and with a green garnet consistent with it having been affected by intense metasomatism including Ca, Fe and Cr (Spengler, 2006). For reasons of comparison to the rest of the pyroxenites we estimated the pre-metasomatic whole-rock composition of this nearly bi-mineralic sample by mixing two appropriate end-member whole rocks from the same peridotite body: the olivine-megacryst DS0212 (42%)

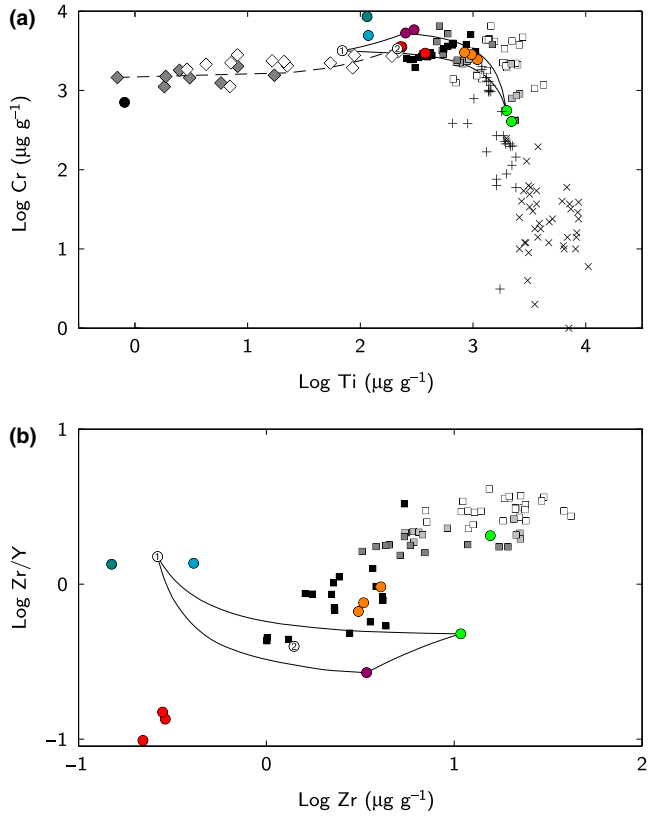

FIGURE 7 Selected whole-rock trace elements of Otrøy mantle rocks (legend as in Figure 5a) and of different mantle volcanics. (a) Cr *v*. Ti. Archean (+; Polat, Hofmann, & Rosing, 2002) and modern (×; Ishizuka et al., 2006; Taylor & Nesbitt, 1998) island arc volcanics have lower Cr at high Ti content compared to Barberton and Commondale komatiite (legend as in Figure 6). Of these, AEK has the highest Cr/Ti, that overlaps Otrøy websterite. The latter forms a mixing relationship with intermediate Cr peridotite (dashed line). (b) Zr/Y *v*. Zr. Different types of South African komatiite (legend as in Figure 6) correlate between Zr content and Zr/Y ratio. The composition of Otrøy garnet-olivine-websterite overlaps that of AEK. The olivine-free variant exceeds the trend to very low values, other pyroxenites and garnetite flank the trend at both sides

and the megacrystalline garnet-orthopyroxenite U95 (58%). The resulting composition model #1 is similar in olivine mode, SiO_2 and MgO contents to those of DS0372, but has lower FeO, Cr and lower CaO/Al_2O_3 (Table S1). The model's Al_2O_3 content, 2.48 wt%, exceeds that of the metasomatic sample, 1.32 wt%.

Another model composition was calculated to test the hypothesis if the three partially olivine-bearing but chemically extreme compositions (orthopyroxenite, garnetite, clinopyroxenite) may be genetically related to each other. The whole rocks of garnet-olivine-orthopyroxenite model #1 (78%), garnetite DS0298 (16%) and garnet-clinopyroxenite DS0295 (6%) were mixed in proportion to meet the REE chemistry of an expected subtype of komatiite (white dashed line in Figure 6a). Related mixing lines of each two of the three end-members are shown in the bivariate chemical diagrams (Figures 5–7) and encircle the model #2 composition. The model #2 major and other trace element contents and ratios were subsequently compared with those of different types of komatiite. All diagrams in the Figures 6 and 7 show our model #2 composition to chemically coincide only with the expected type of komatiite. This coincidence supports the chemically extreme rock types not only to have a shared origin but also that this origin is related to that of the websterites. The details are discussed in the following subsection.

4.3 | Origin of pyroxenite

The MgO–SiO_2 systematics of the Otrøy pyroxenites differ to those of rocks that are expected to form by re-equilibration between melt-depleted peridotite and infiltrated silica-rich fluids or melts (Figure 5b). Instead, the contents and ratios of these major element oxides in Otrøy websterite are consistent with those of komatiite flows from Barberton and Commondale Greenstone belts, South Africa, including spinifex, massive and cumulate subtypes of komatiite (shaded field in Figure 5b; Hoffmann & Wilson, 2017; Robin-Popieul et al., 2012; Thompson Stiegler, Lowe, & Byerly, 2010; Wilson, 2003). Therefore, we regard the websterites as being crystallized from dense melts at depth. Compositions of the other three, partially olivine-bearing and partially nearly monomineralic types of pyroxenite and garnetite lie on opposite sides of the komatiite array in Figure 5b. Undeformed representatives of these rock types occur solely as isolated fragments (Carswell, 1973; Van Roermund, 2009; Van Roermund & Drury, 1998) with an unclear spatial relationship with each other. Although, the extreme whole-rock chemistry of each of the three rock types, that is, Ca-Al-rich *v*. Al-rich *v*. Mg-Si-rich, suggests that clinopyroxenite, garnetite and orthopyroxenite represent fragments of a mineralogically stratified precursor pyroxenite. Such a hypothetical composite rock (triangular mixing field in Figure 5b) has large compositional overlap with the komatiite array that includes the specific model #2 composition. In addition, the model #2 websterite consists of all major minerals present in Otrøy garnet-olivine-websterite. A shared origin of websterite and the other pyroxenitic rocks is further supported by microstructures, that is, the presence of oriented pyroxene lamellae in garnet cores after majorite garnet precursors in all four (non-metasomatic) rock types (Spengler, 2006; Spengler et al., 2009; Van Roermund & Drury, 1998), and by a 3.33 ± 0.19 Ga whole-rock isochron relationship between different pyroxenites (Spengler et al., 2009). Direct evidence of such composite precursor pyroxenite prior to major peridotite deformation is provided by rare m-scale pyroxenite lenses that contain clusters of garnetite in garnet-orthopyroxenite (Brueckner, Carswell, & Griffin, 2002; Carswell, 1973).

To be recognized as mantle melts or as parts of mantle melts, the pyroxenites should lack major chemical substitution with the peridotites. This precondition is demonstrated by the mineral chemistry. Garnet grains that have been mixed into peridotite (n = 7) have $Mg^{\#}$ of 0.78–0.84 (median 0.81; Spengler, 2006). Those of garnet in garnetite (n = 3) are higher, 0.86–0.89 (median 0.86), and those of garnet in the pyroxenites (n = 7) are lower, 0.66–0.81 (median 0.74; Spengler, 2006; Spengler et al., 2009). These characteristics suggest that chemical re-equilibration of fast diffusing elements like Fe was efficient with respect to single garnet grains when in contact with peridotite, but was inefficient at the whole-rock scale. Similarly, accessory olivine in garnetite (n = 2) has $Mg^{\#}$ of 0.95 (Spengler et al., 2006; Van Roermund et al., 2000) in contrast to peridotitic olivine (n = 10) with $Mg^{\#}$ of 0.92–0.93 (Spengler, 2006), again highlighting the chemical dis-equilibrium at whole-rock scale. In addition, the olivine-bearing pyroxenites have porphyroclastic minerals with olivine inclusions that demonstrate the presence of olivine in this group of pyroxenites during crystallization prior to deformation (Figure 4).

The pyroxenite major and REE chemistry further supports a komatiitic signature. Komatiite liquids are defined by a high MgO content, 18–30 wt% (Arndt & Lesher, 2005). Dependent on variable sources and degrees of melting, komatiites are commonly subdivided into three major types, that is, Al-depleted ($Al_2O_3/TiO_2 \sim 10$), Al-undepleted ($Al_2O_3/TiO_2 \sim 20$) and Al-enriched (Al_2O_3/TiO_2 >25) komatiite (ADK, AUK and AEK respectively; Arndt & Lesher, 2005; Robin-Popieul et al., 2012). Characteristics of komatiitic suites include a negative correlation of Al_2O_3/TiO_2 with the depletion and fractionation of REE (Figure 6a–c). As a function of their extents, we distinguish two subtypes of AEK: moderately depleted AEK and extremely depleted AEK (dark grey and black shaded fields and symbols in Figure 6 respectively). Otrøy websterite has a MgO content of 22.7–29.0 wt% (Table S1), Al_2O_3/TiO_2 of 19.5–94.7 and fractionated heavy REE with Gd_N/Yb_N of 0.49–0.85, chemical characteristics that are comparable to those of AEK (Figure 6c). In addition, REE, TiO_2 and Al_2O_3 contents of Otrøy websterites are nearly indistinguishable from those of AEK from Barberton and Commondale (Figure 6a,b). Websterite samples from the Midsundvatnet body (all are olivine-bearing) have moderate Al_2O_3/TiO_2 (19.5–27.9) and moderate Gd_N/Yb_N (0.73–0.85) that resemble the chemistry of moderately depleted AEK. In contrast, websterite from the other two bodies on Otrøy (i.e. olivine-free) is chemically similar to the extreme subtype of AEK (40.4–94.7 and 0.49–0.65 respectively).

Not surprisingly, Ugelvik and Raudhaugene clinopyroxenite, orthopyroxenite and garnetite chemically differ. Bivariate plots show that the compositions of these three rock types define mixing lines and fields that—irrespective of whether olivine is compositionally included (using model #1) or not (using sample U95)—enclose Ugelvik and Raudhaugene websterite only partially (Figures 6b,c and 7). For example, variation in proportion of the rock triplet's components does not reconcile the garnet-websterite's high CaO/Al_2O_3 ratio and low Zr content. The model #2 websterite, however, overlaps nearly perfectly with all chemical characteristics of the extreme subtype of AEK (Figures 6 and 7). This relationship further supports the rock triplet of (model) garnet-olivine-orthopyroxenite, garnetite and garnet-clinopyroxenite to represent now isolated components of a formerly komatiitic precursor websterite with modal heterogeneity that hardly survived major deformation of the peridotite.

Deviation in chemistry of olivine-free websterite to AEK (extreme subtype) includes slightly higher Al_2O_3/TiO_2 for a given Gd_N/Yb_N, clearly higher CaO/Al_2O_3 and clearly lower Zr and Zr/Y (Figures 6c,d and 7b). Similar variations are recorded in the AEK moderate subtype data set. For example, the three samples of the latter with the highest CaO/Al_2O_3 (sample numbers MC5-6, WP105 and WP108) range 1.5–2.8 that is similar to that of Otrøy garnet-websterite, 1.5–2.6. The same samples from South Africa have slightly higher Al_2O_3/TiO_2 for a given Gd_N/Yb_N as do the Otrøy samples (Figure 6c). The former show either pyroxene cumulate or pyroxene spinifex textures and may therefore be regarded as being formed from evolved liquids. Consistently, their Zr content, 5–19 μg/g, includes the highest values in the data subset. On the contrary, the Zr content in Otrøy garnet-websterite is very low, 0.22–0.29 μg/g. Experimental liquid/mineral partition data for Zr in clinopyroxene and garnet, the two major host phases for Zr in Otrøy garnet-websterite, increase beyond unity with increasing mantle temperature greater 1,000°C (Stalder, Foley, Brey, & Horn, 1998). Hence, very low Zr in garnet-websterite may be indicative for both a high-T mantle process and that these samples have crystallized from a melt that may have migrated further (cumulate origin at high pressure and temperature). The absence of olivine, one of the first mineral phases expected to crystallize from an ultramafic melt, in these samples suggest the parental melt to have already been evolved, in turn consistent with high CaO/Al_2O_3 in garnet-websterite. The Zr content in the other, olivine-bearing websterites (model #2 and measured) is as low as in the cumulate surface counterparts (Figure 7b), which suggests the former to have formed at depth in a similar fashion.

Solidified surface flows of komatiite liquids record crystallization conditions over a large range of thermal gradients that caused formation of different textures and of chemical fractionation series. All of them share the same source, an individual komatiite liquid and so are termed komatiite.

Texturally, the Otrøy pyroxenites have primary crystal sizes that exceed those of surface cumulates as is to be expected from low thermal gradients during crystallization at depth. The remarkable similarity in chemistry of the studied pyroxenites and AEK suggests that the pyroxenites represent depth equivalents of the AEK. These plutonic equivalents do not necessarily need to represent primary komatiite melts, but appear to have crystallized from primary or more evolved liquids or both, including cumulate processes.

4.4 | Extent and depth of melting

Previous studies have demonstrated that komatiitic melts that are depleted in melt-compatible elements but relatively enriched in melt-incompatible heavy REE are formed by melting of a garnet-bearing peridotite that has been previously melt depleted (Herzberg, 1995). Initial low degree melting of peridotite (18%) would first form ADK (Sproule, Lesher, Ayer, Thurston, & Herzberg, 2002) within the stability field of garnet in peridotite. Subsequent high degree melting (28%) of the garnet-enriched residue would form AEK (Sproule et al., 2002). The total discharge of melt from both melting sequences (46%) is consistent with the melt depletion recorded in the major element oxides of Otrøy spinel-peridotite (40–55%) that hosts the komatiitic websterites.

The geodynamic implication of the geochemical variations depends on the liquid crystallization depth that provides a conservative estimate for the depth of melting. Lamellae type pyroxene exsolution microstructures with a maximum of 1–1.5 vol.% pyroxene after former majoritic garnet are recorded in all types of Otrøy garnet-pyroxenite and garnetite that are unaffected by Ca–Cr–Fe metasomatism (Figure 4c; Spengler, 2006; Spengler et al., 2009; Van Roermund & Drury, 1998). This observation indicates solidus crystallization temperatures exceeding 1,600°C for these rocks (Gasparik, 2014). A crystallization pressure of 3.1–3.8 GPa is derived from the intersection of the pyroxenite solidus with Si isopleths in garnet (Gasparik, 2014). A fundamental consequence of this observation is that mantle melting of $\sim$50% at $\sim$100 km depth and at such high temperatures requires a major thermal anomaly and can only be explained by a mantle plume scenario (Arndt et al., 2009; Herzberg, 1995). Furthermore, the exsolved mineral chemistry records comparable pressures, weighted mean 3.6 $\pm$ 0.1 GPa, and an equilibration of the pyroxenites at a cratonic geotherm with 37 mW/m^2 surface heat flow (Spengler et al., 2009). It follows that pyroxenite crystallization at high temperatures, subsequent exsolution of pyroxene lamellae in garnet and finally mineral chemical equilibration at low temperatures occurred at the same depth level, which indicates a long-term stability of these mantle fragments prior to their Caledonian tectonometamorphic overprint. An inference of this scenario is that Otrøy websterite formed by dry peridotite melting. These high-*P* and high-*T* melts with relatively high Cr content, 2,450–3,560 μg/g, chemically differ from mantle melts presumably formed by hydrous melting at lower pressure and temperature that typically have low Cr content, 1–1,920 μg/g (Figure 7a).

5 | CONCLUSIONS AND IMPLICATIONS

In summary, the Otrøy peridotite bodies record extreme melting temperatures, high fractions of melt extracted in the garnet-peridotite field and enclose pyroxenites that witness Al-enriched komatiitic melts to have partially refertilized the residua in the garnet-peridotite field during the Palaeoarchean. These characteristics are expected for Archean plume heads. Such plume heads (or large igneous plateaus) are buoyant compared to residues that formed at Archean spreading centres, and therefore are unlikely to be subducted or recycled into the convecting mantle. We suggest that the initial stage of cratonization of the eastern Rae craton was triggered by the formation and assembly of buoyant lithosphere above plume heads, before periods of vertical growth by tectonic and/or other mantle processes have led to the cratonic mantle architecture as can be seen today.

ACKNOWLEDGEMENTS

G. Davies is thanked for the supervision of the MSc projects of Z. Vukmanović and E. Wiersma and for his constructive and critical comments to the very first version of this manuscript. We appreciate the sceptic but crucial remarks from C. Herzberg and N. Arndt that led to an overall improvement and D. Robinson for his thoughtful suggestions and editorial handling.

REFERENCES

Arndt, N. T., Coltrice, N., Helmstaedt, H., & Gregoire, M. (2009). Origin of Archean subcontinental lithospheric mantle: Some petrological constraints. *Lithos*, *109*, 61–71. https://doi.org/10.1016/j.lithos.2008.10.019

Arndt, N. T., & Lesher, C. M. (2005). Komatiite. In R. C. Selley, L. R. M. Cocks & I. R. Plimer (Eds.), Encyclopedia of geology (vol. 3, pp. 260–267). Oxford: Elsevier. https://doi.org/10.1016/B0-12-369396-9/00297-5

Brueckner, H. K. (1998). Sinking intrusion model for the emplacement of garnet-bearing peridotites into continent collision orogens. *Geology*, *26*(7), 631–634. https://doi.org/10.1130/0091-7613(1998)026<0631:SIMFTE>2.3.CO;2

Brueckner, H. K., Carswell, D. A., & Griffin, W. L. (2002). Paleozoic diamonds within a Precambrian peridotite lens in UHP gneisses of the Norwegian Caledonides. *Earth and Planetary Science Letters*, *203*, 805–816. https://doi.org/10.1016/S0012-821X(02)00919-6

Carswell, D. A. (1973). Garnet pyroxenite lens within Ugelvik layered garnet peridotite. *Earth and Planetary Science Letters*, *20*, 347–352. https://doi.org/10.1016/0012-821X(73)90009-5

Carswell, D. A., Van Roermund, H. L. M., & Wiggers de Vries, D. F. (2006). Scandian ultrahigh-pressure metamorphism of Proterozoic basement rocks on Fjørtoft and Otrøy, Western Gneiss Region, Norway. *International Geology Review*, *48*(11), 957–977. https://doi.org/10.2747/0020-6814.48.11.957

Gasparik, T. (2014). Phase diagrams for geoscientists – An atlas of the earth's interior (2nd ed.). New York, NY: Springer. https://doi.org/10.1007/978-1-4614-5776-3

Herzberg, C. (1995). Generation of plume magmas through time: An experimental perspective. *Chemical Geology*, *126*, 1–16. https://doi.org/10.1016/0009-2541(95)00099-4

Herzberg, C. (2004). Geodynamic information in peridotite petrology. *Journal of Petrology*, *45*(12), 2507–2530. https://doi.org/10.1093/petrology/egh039

Herzberg, C., Condie, K., & Korenaga, J. (2010). Thermal history of the Earth and its petrological expression. *Earth and Planetary Science Letters*, *292*, 79–88. https://doi.org/10.1016/j.epsl.2010.01.022

Herzberg, C., & Rudnick, R. (2012). Formation of cratonic lithosphere: An integrated thermal and petrological model. *Lithos*, *149*, 4–15. https://doi.org/10.1016/j.lithos.2012.01.010

Hoffmann, J. E., & Wilson, A. (2017). The origin of highly radiogenic Hf isotope compositions in 3.33 Ga Commondale komatiite lavas (South Africa). *Chemical Geology*, *455*, 6–21. https://doi.org/10.1016/j.chemgeo.2016.10.010

Ishizuka, O., Kimura, J.-I., Li, Y. B., Stern, R. J., Reagan, M. K., Taylor, R. N., & Haraguchi, S. (2006). Early stages in the evolution of Izu-Bonin arc volcanism: New age, chemical, and isotopic constraints. *Earth and Planetary Science Letters*, *250*, 385–401. https://doi.org/10.1016/j.epsl.2006.08.007

Komiya, T., Maruyama, S., Hirata, T., Yurimoto, H., & Nohda, S. (2004). Geochemistry of the oldest MORB and OIB in the Isua Supracrustal Belt, southern West Greenland: Implications for the composition and temperature of early Archean upper mantle. *Island Arc*, *13*(1), 47–72. https://doi.org/10.1111/j.1440-1738.2003.00416.x

Kretz, R. (1983). Symbols for rock-forming minerals. *American Mineralogist*, *68*, 277–279.

McDonough, W. F., & Sun, S.-S. (1995). The composition of the earth. *Chemical Geology*, *120*, 223–253. https://doi.org/10.1016/0009-2541(94)00140-4

Pearson, D. G., & Wittig, N. (2008). Formation of Archaean continental lithosphere and its diamonds: The root of the problem. *Journal of the Geological Society*, *165*(5), 895–914. https://doi.org/10.1144/0016-76492008-003

Polat, A., Hofmann, A. W., & Rosing, M. T. (2002). Boninite-like volcanic rocks in the 3.7–3.8 Ga Isua greenstone belt, West Greenland: Geochemical evidence for intra-oceanic subduction zone processes in the early Earth. *Chemical Geology*, *184*, 231–254. https://doi.org/10.1016/S0009-2541(01)00363-1

Robin-Popieul, C. C. M., Arndt, N., Chauvel, C., Byerly, G. R., Sobolev, A. V., & Wilson, A. (2012). A new model for Barberton komatiites: Deep critical melting with high melt retention. *Journal of Petrology*, *53*(11), 2191–2229. https://doi.org/10.1093/petrology/egs042

Simon, N. S. C., Carlson, R. W., Pearson, D. G., & Davies, G. R. (2007). The origin and evolution of the Kaapvaal cratonic lithospheric mantle. *Journal of Petrology*, *48*(3), 589–625. https://doi.org/10.1093/petrology/egl074

Spengler, D. (2006). *Origin and evolution of deep upper mantle rocks from western Norway*, PhD Thesis. Geologica Ultraiectina, 266. Retrieved from http://igitur-archive.library.uu.nl/dissertations/2006-1114-200554/index.htm

Spengler, D., Brueckner, H. K., van Roermund, H. L. M., Drury, M. R., & Mason, P. R. D. (2009). Long-lived, cold burial of Baltica to 200 km depth. *Earth and Planetary Science Letters*, *281*, 27–35. https://doi.org/10.1016/j.epsl.2009.02.001

Spengler, D., Obata, M., Hirajima, T., Ottolini, L., Ohfuji, H., Tamura, A., & Arai, S. (2012). Exsolution of garnet and clinopyroxene from high-Al pyroxenes in Xugou peridotite, eastern China. *Journal of Petrology*, *53*(7), 1477–1504. https://doi.org/10.1093/petrology/egs023

Spengler, D., Van Roermund, H. M. L., Drury, M. R., Ottolini, L., Mason, P. R. D., & Davies, G. R. (2006). Deep origin and hot melting of an Archaean orogenic peridotite massif in Norway. *Nature*, *440*, 913–917. https://doi.org/10.1038/nature04644

Sproule, R. A., Lesher, C. M., Ayer, J. A., Thurston, P. C., & Herzberg, C. T. (2002). Spatial and temporal variations in the geochemistry of komatiites and komatiitic basalts in the Abitibi greenstone belt. *Precambrian Research*, *115*, 153–186. https://doi.org/10.1016/S0301-9268(02)00009-8

Stalder, R., Foley, S. F., Brey, G. P., & Horn, I. (1998). Mineral-aqueous fluid partitioning of trace elements at 900–1200 °C and 3.0–5.7 GPa: New experimental data for garnet, clinopyroxene, and rutile, and implications for mantle metasomatism. *Geochimica et Cosmochimica Acta*, *62*(10), 1781–1801. https://doi.org/10.1016/S0016-7037(98)00101-X

St-Onge, M. R., Van Gool, J. A. M., Garde, A. A., & Scott, D. J. (2009). Correlation of Archaean and Palaeoproterozoic units between northeastern Canada and western Greenland: Constraining the pre-collisional upper plate accretionary history of the Trans-Hudson orogen. *Geological Society, London, Special Publications*, *318*, 193–235. https://doi.org/10.1144/SP318.7

Sun, S. S. (1982). Chemical composition and origin of the earth's primitive mantle. *Geochimica et Cosmochimica Acta*, *46*, 179–192. https://doi.org/10.1016/0016-7037(82)90245-9

Sun, S.-S., & McDonough, W. F. (1989). Chemical and isotopic systematics of oceanic basalts: Implications for mantle composition and processes. *Geological Society, London, Special Publications*, *42*, 313–345. https://doi.org/10.1144/GSL.SP.1989.042.01.19

Taylor, R. N., & Nesbitt, R. W. (1998). Isotopic characteristics of subduction fluids in an intra-oceanic setting, Izu-Bonin Arc, Japan. *Earth and Planetary Science Letters*, *164*, 79–98. https://doi.org/10.1016/S0012-821X(98)00182-4

Thompson Stiegler, M., Lowe, D. R., & Byerly, G. R. (2010). The petrogenesis of volcaniclastic komatiites in the Barberton greenstone belt, South Africa: A textural and geochemical study. *Journal of Petrology*, *51*(4), 947–972. https://doi.org/10.1093/petrology/egq008

Van Roermund, H. L. M. (2009). Mantle-wedge garnet peridotites from the northernmost ultra-high pressure domain of the Western Gneiss

Region, SW Norway. *European Journal of Mineralogy*, *21*, 1085–1096. https://doi.org/10.1127/0935-1221/2009/0021-1976

Van Roermund, H. L. M., & Drury, M. R. (1998). Ultra-high pressure (P > 6 GPa) garnet peridotites in western Norway: Exhumation of mantle rocks from >185 km. *Terra Nova*, *10*(6), 295–301. https://doi.org/10.1046/j.1365-3121.1998.00213.x

Van Roermund, H. L. M., Drury, M. R., Barnhoorn, A., & De Ronde, A. A. (2000). Super-silicic garnet microstructures from an orogenic garnet peridotite, evidence for an ultra-deep (>6 GPa) origin. *Journal of Metamorphic Geology*, *18*(2), 135–147. https://doi.org/10.1046/j.1525-1314.2000.00251.x

Walter, M. J. (1998). Melting of garnet peridotite and the origine of komatiite and depleted lithosphere. *Journal of Petrology*, *39*(1), 29–60. https://doi.org/10.1093/petroj/39.1.29

Walter, M. J. (2003). Melt extraction and compositional variability in mantle lithosphere. In H. D. Holland & K. K. Turekian (Eds.), Treatise on geochemistry (Vol. 2: The Core and Mantle, pp. 363–394). Oxford: Elsevier. https://doi.org/10.1016/B0-08-043751-6/02008-9

Wilson, A. H. (2003). A new class of silica enriched, highly depleted komatiites in the southern Kaapvaal Craton, South Africa. *Precambrian Research*, *127*, 125–141. https://doi.org/10.1016/S0301-9268(03)00184-0

SUPPORTING INFORMATION

Additional supporting information may be found online in the Supporting Information section at the end of the article.

Table S1. Major and trace element concentrations of Otrøy pyroxenite and garnetite and calculated mineral modes

Table S2. Major and trace element concentrations of Otrøy peridotite and calculated mineral modes

Table S3. Major element concentrations (wt.%) in mineral cores of Otrøy pyroxenite and garnetite

Table S4. Trace element concentrations (μg/g) of minerals in Otrøy pyroxenite

How to cite this article: Spengler D, van Roermund HLM, Drury MR. Deep komatiite signature in cratonic mantle pyroxenite. *J Metamorph Geol*. 2018;36:591–602. https://doi.org/10.1111/jmg.12310